Impacts of a new Solar Radiation Parameterization on the CPTEC AGCM Climatological Features

H.M.J. Barbosa[*], T.A. Tarasova[†]and I.F.A. Cavalcanti

Centro de Previsão de Tempo e Estudos Climáticos, Cachoeira Paulista, SP, Brasil

[*]*Corresponding author address:* Dr. Henrique Barbosa, Centro de Previsão de Tempo e Estudos Climáticos,

Rodovia Presidente Dutra, Km 40, 12630-000, Cachoeira Paulista, SP, Brasil.

E-mail: hbarbosa@cptec.inpe.br

[†]Additional Affiliation: Institute of Atmospheric Physics, Russian Academy of Sciences, Moscow, Russia.

Abstract

We investigate the impacts of an improved atmospheric absorption on radiative fluxes, atmospheric circulation and hydrological cycle for long-term GCM integrations. For these runs we use the operational version of the CPTEC AGCM and its enhanced version with a new solar radiation scheme. There is an 8% increase in the annual mean global average atmospheric absorption in the enhanced integration as compared with the operational model integration. The extra absorption is due to gases (0.5%), water vapor continuum (1.5%) and background aerosols (6%), which were not considered in the operational solar radiation scheme. In clear-sky conditions the enhanced model atmospheric absorption is in agreement with observations to within ± 3 W/m^2, while in all-sky conditions the remaining errors are related to unaccounted cloud absorption. There is a general warm up of the atmosphere in the enhanced model with temperatures increasing up to $\sim$3K in the troposphere and $\sim$5–8K in the stratosphere, bringing the model closer to reference values. The intensity of the tropospheric jets is reduced by 7–8%, while that of the polar night stratospheric jet are increased by 5-10%, reducing the model systematic error. The reduced availability of latent energy for the saturated convective processes weakens the meridional circulation and slows down the hydrological cycle. The model overestimation of DJF precipitation over the SPCZ and SACZ regions is reduced by 0.5–1.0 mm day^{-1} and over the northern hemisphere storm tracks region by 0.5 mm day^{-1}. In the monthly time scale, the changes on the precipitation distribution over the SACZ region are found to be much larger $\pm$ 2–3mm day^{-1}.

1

1. Introduction

General circulation models are used in climate simulations to study climate variability, climate change, and for seasonal forecasting. For all these applications, it is crucial that a model simulates well the observed climate and its variability. In this sense, results of long-term integrations are used to show the ability of different models in representing observed characteristic features of the atmospheric circulation and precipitation (Hurrell et al. 1998; Gates et al. 1999; Johns et al. 1997; Pope et al. 2000). These are important to provide a model climatology and to perform model validation, giving confidence for its applicability. Long-term integrations are also used for comparing different climate models (Atmospheric Model Intercomparison Project, AMIP: Gates 1992; Gates et al. 1999). The comparison of GCMs shows that they overestimate by 20-42 W/m^2 the global net surface insolation when compared with ground measurements (Wild et al. 1995; Wild and Ohmura 1999; Wild 2005) and satellite derived surface solar radiative fluxes (Cess et al. 1995; Li et al. 1999; Cusack et al. 1998; Tarasova and Cavalcanti 2002).

If the systematic errors in the global net surface insolation from GCMs are reduced or eliminated, the effects on atmospheric and oceanic circulations are substantial (Kiehl 1994). For instance, an additional shortwave absorption in the tropical atmosphere by 25 W/m^2 increases the meridional transport of moist static energy by approximately 50% (Kiehl 1994). Moreover, as the terms for insolation and latent heat flux dominate the heat balance of the tropical oceans (Monin 1986), the latent heat flux has to decrease by roughly the same as the surface insolation to maintain the energy balance. This corresponding reduction of evaporation significantly affects the state of the tropical troposphere (Kiehl et al. 1995), reducing the convectively available potential energy and decelerating the Walker circulation and hydrological cycle (Collins 2006).

2

However, there is not an agreement about the magnitude of the changes in the temperature and wind fields, nor in the hydrological cycle.

In the early 90's, Hart et al. (1990) used the Australian Bureau of Meteorology Research Centre (BMRC) spectral model to demonstrate the impact of changes in physical parameterizations on perpetual January and July integrations. They found, for the runs with an enhanced radiation scheme, that winter stratosphere temperature cool bias was reduced from -30K to less than -20K. Moreover, there was a significant improvement in the intensity of the polar night jet, that showed a clear separation from the tropospheric jet. However, Hart et al. (1990) noticed that a good description of the upper troposphere and stratosphere zonal wind and temperatures depend not only on the radiative processes but also on the deep and shallow convection, vertical diffusion and horizontal resolution.

Morcrette (1990) evaluated the impact of improvements in the radiation and in-cloud properties upon the climate of the ECMWF model. Differently from other GCMs, the ECMWF model used to overestimate the atmospheric absorption of solar radiation by 15–20% and underestimate the longwave cooling by 10–15%. By replacing the radiation scheme, Morcrette found that the bias of atmospheric absorption of solar radiation reduced to less than +5% while the meridional circulation and hydrological cycle, i.e. both precipitation and evaporation, became 15% stronger.

More recent studies investigated the response of GCMs to smaller updates in the radiation schemes and hence found weaker response of the hydrological cycle. For instance, to study the climatic effects of an improved atmospheric absorption Lohmann and Bennartz (2002) integrated ECHAM4 with two water vapor broad band absorption functions, based on the HITRAN-92 and HITRAN-2K (Rothman et al. 2003) molecular absorption databases. They found that the

global-mean atmospheric shortwave absorption increased by 3.2–3.7 W/m^2 while the surface insolation decreased by 2.1–2.5 W/m^2. As a consequence of the increased atmospheric stability and the reduction in surface fluxes, the hydrological cycle decreased slightly in strength, with a reduction in the global precipitation of 0.07 mm day^{-1}.

Collins et al. (2006) did a similar study using the Community Atmospheric Model (CAM). The original water vapor broad band absorption function (Briegleb 1992), based on the 1982 AFGL molecular absorption database of Rothman et al. (1983), was updated to a function based on the HITRAN-2K database (Rothman et al. 2003). The absorption by the water vapor continuum (Clough et al. 2005) was also included. They found that the atmospheric absorption increased by 3.4 W/m^2 while the surface insolation decreased by 2.8 W/m^2. Moreover, the change in the surface insolation was balanced primarily by a reduction of the latent heat and the hydrological cycle was weakened by 2% (global precipitation falls by 0.05 mm day^{-1}).

Other studies have changed the atmospheric absorption in the cloudy atmosphere only, trying to model the enhanced shortwave absorption observed in cloudy conditions. Kiehl et al. (1995) modified the NCAR Community Climate Model (CCM2) to increase the cloud absorption through ad-hoc changes in the single-scattering albedo of cloud particles. They found that the extra absorption stabilized the tropical convective atmosphere and caused a 3–4K warming of the upper tropical troposphere. The increased stability reduced the convective activity and resulted in a weaker Walker circulation.

In a similar study, Collins (2006) modified the absorption effect of clouds by empirically changing the vertical profiles of heating rates in the NCAR Climate System Model (CSM). He found that the upper tropical troposphere temperature increased as much as 5K near 100hPa, due to the increase of the all-sky heating rates by as much as 1K/day at the same altitude. As a

consequence of the new vertical profile of temperature, the cloud cover decreased by 10–15% at high levels and increased by 5–15% at middle and low levels. At the same time, the latent heat flux over the tropical western Pacific reduced by as much as 20-40 W/m^2.

The CPTEC AGCM is used for weather and climate forecast at the Brazilian Center for Weather Forecast and Climate Studies (CPTEC). It is a new Global Eulerian Spectral model (see section 2) based on the CPTEC/COLA (Center for Ocean-Land-Atmosphere Studies) GCM described by Cavalcanti et al. (2002). To improve the model surface flux representation the k-distribution formulation for water vapor solar absorption of Davies (1982) was replaced by Ramaswamy and Freidenreich (1992). Chagas et al. (2004) found some minor improvements in the surface fluxes, with a reduction in the bias of the all-sky surface flux from +20 W m^{-2} to +16 W m^{-2} (yearly averages for one 20 year integration).

In order to further improve the atmospheric absorption of solar radiation by gases and aerosols, a sophisticated shortwave radiation scheme developed by Chou and Suarez (1999) and modified by Tarasova and Fomin (2000), referenced later as *CLIRAD-SW-M*, was implemented by Tarasova et al. (2006) the CPTEC/COLA model. This scheme considers the fine effects of gaseous absorption and particle scattering which were not considered in previous versions of the CPTEC/COLA model. The modified code *CLIRAD-SW-M* also takes into account the water vapor continuum absorption model proposed by Clough et al. (1989). Tarasova et al. (2006) did an initial validation of the new scheme outside the framework of the global model and showed that the differences between *CLIRAD-SW-M* and line-by-line (LBL) reference results of Fomin and Gershanov (1996) were of the order of 1-2 W/m^2 for clear-sky, and 6 W/m^2 for cloudy atmospheres. They also integrated the global model for the DJF 2002/3 and found that the surface fluxes were significantly improved over South America. In particular, the ex-

5

cessive solar radiation biases at the surface were reduced from 30–80 W/m^2 to 10–30 W/m^2. As compared with GPCP data (GPCP v2: Adler et al. 2003) the model-simulated magnitude of precipitation was improved over equatorial Atlantic Ocean and Southeastern Brazil.

This paper reports the improvements achieved with the new shortwave radiation scheme on the radiation balance, the atmospheric circulation and hydrological cycle of the new CPTEC AGCM. The impacts on the hydrological cycle are studied over different time scales and the sources of the differences between the new model and observations are investigated. For evaluating the model's sensitivity to each of the changes in the solar radiation absorption, we introduce the changes one-by-one and compare the model results with satellite derived observations and NCEP Reanalysis. Our results are particularly relevant to the ongoing investigation on the global climate response due to changes in the shortwave absorption of the atmosphere, either to correct model biases or to simulate future loadings of aerosol and green house gases.

This paper is divided as follows: section 2 gives a brief description of the CPTEC model and the new shortwave radiation scheme. The experiment design and data used for model validation are given in section 3. Section 4 is devoted to the comparison of the model climatology and observations, while section 5 presents the discussion. Conclusions and future perspectives are presented in section 6.

2. Short description of the CPTEC AGCM

The CPTEC AGCM is a Global Eulerian Spectral model which is based on the CPTEC/COLA model (Cavalcanti et al. 2002). This new model is operational since 2004. An overview of the global climate simulated with the CPTEC/COLA model is given by Cavalcanti et al. (2002).

They have shown that the model simulates reasonably well the main features of global climate, as well as the seasonal variability of the main atmospheric variables. The most important difference between the original CPTEC/COLA model and the currently operational CPTEC model is a change in the water vapor solar radiation absorption (Chagas et al. 2004). Other modifications are related to its computer efficiency and do not change the model climatological features.

The model physical processes include the vegetation module Simple Surface Biosphere Model (Xue et al. 1991, SSIB:); second-order closure turbulent vertical diffusion following Mellor and Yamada (1982); shallow cumulus effects following Tiedtke (1984); Kuo (1974), Anthes (1977) deep cumulus convection scheme; large scale precipitation produced from removal of supersaturation; longwave radiation following the work of Harshvardhan and Corsetti (1984), including the scheme of Harshvardhan et al. (1987) to include the diurnal cycle; and the cloud-radiation interaction of Slingo (1987) and Hou (1990).

a. The Operational SW Scheme

The operational shortwave scheme follows the parameterizations of Lacis and Hansen (1974) with the eleven-exponential-term k-distribution formulation of Ramaswamy and Freidenreich (1992) which replaced the k-distribution formulation of Davies (1982) originally used in the CPTEC/COLA model. This replacement improved the heating rate profiles (Plana-Fattori et al. 1997) and the surface fluxes (Chagas et al. 2004). Nonetheless, this scheme only takes into account the absorption lines of H_2O and O_3, Rayleigh scattering and cloud reflection, neglecting atmospheric extinction due to O_2, CO_2, aerosols and water vapor continuum. The solar radiation absorption by water vapor is computed with the broadband absorption function of Yamamoto (1962) which underestimates the water vapor absorption when compared with the HITRAN-96

7

spectroscopic database of Rothman et al. (1998).

b. The New SW Scheme

The new shortwave scheme *CLIRAD-SW-M* is a modified version of the parameterization of Chou and Suarez (1999). The code was modified by Tarasova and Fomin (2000) to take into account the water vapor continuum absorption model proposed by Clough et al. (1989). This was done by changing the water vapor k-distribution functions in the near-infrared bands. The magnitude of the continuum absorption is about 6% of the water vapor line absorption. The new scheme includes the absorption due to major and minor absorption bands of H_2O, O_3, O_2 and CO_2. The magnitude of the absorption in the minor bands is small, but the total effect is large, about 10% of the column atmospheric heating. Absorption lines of gases and absorption and scattering properties of aerosols and cloud particles are taken from the HITRAN-96 molecular absorption database (Rothman et al. 1998). The code has 8 spectral bands in the ultraviolet and visible regions of the solar spectrum and 3 bands in the near infrared region. The solar radiative transfer is calculated with the delta-Eddington and two-stream adding approximations.

Aerosol optical properties are specified as inputs to the scheme. As the CPTEC AGCM lacks prognostic aerosol amounts and size distributions, we introduced a basic climatology of background aerosols. At each grid point we chose from two aerosol loadings, namely continental and oceanic. The continental aerosol has a column optical depth of 0.22, homogeneously distributed in the first 2 km of the atmosphere, and is chosen over all land points except those with permanent ice. The value of 0.22 is derived from recent satellite measurements taken over the continents (Yu et al. 2006). It describes average aerosol loading over the continents far from strong sources of aerosol emission such as biomass burning. Similarly, the oceanic aerosol has a

8

column optical depth of 0.14 (Yu et al. 2006) and is chosen over ocean and sea ice. The spectral variations of aerosol optical parameters follow the continental and oceanic aerosol types from (World Meteorological Organization 1986). This prescription has rough spatial and temporal resolutions, but allows for first-order effects of aerosols to be considered.

Tarasova et al. (2006) did an offline validation of the new scheme using as reference a state-of-art LBL method. They showed that the accuracy of the *CLIRAD-SW-M* scheme is superior to the previous schemes for both incident solar radiation and atmospheric absorption. For clear sky atmospheres, *CLIRAD-SW-M* corrected completely the systematic error for the midlatitude summer standard atmosphere and reduced it to the order of 1 to 2 $\mathrm{W\,m^{-2}}$ for the tropical atmosphere in clear-sky conditions. It was also shown that for cloudy atmospheres the systematic differences from the LBL results were reduced to 6 to 8 $\mathrm{W\,m^{-2}}$.

3. Model Experiment and Data used for Validation

Global climatology is simulated integrating the model for 10 years, from January 1985 to December 1994. To gain greater sample diversity and statistical significance, an ensemble mode is used in which integrations start from 4 different days, between 13 and 16 November 1984. To investigate the model sensitivity to the changes in the radiation, three sets of model integrations with the new shortwave scheme (hereafter NEW model) were carried out. In the first set of integrations, the NEW model is used including all features of the sw scheme described in the section 2b, i.e., background aerosols scattering and absorption and water vapor continuum absorption (hereafter NEW model results). In the second set the background aerosols effect was removed (hereafter N-A results). In the third set both the aerosols and the water vapor

continuum effects were removed (hereafter N-WA results). A set of model integrations with the operational shortwave scheme (hereafter OPE model results) is used as a control.

The model resolution used for these climatic simulations is T62 L28, corresponding to a triangular truncation of 62 waves in the horizontal and 28 levels in the vertical sigma coordinate, with time steps of 20 minutes. The initial conditions are from the 12Z daily analysis of the National Centers for Environmental Prediction/National Center for Atmospheric Research (NCEP-NCAR). A monthly climatology of soil moisture and temperature are interpolated to the initial condition time and adjusted during integration by SSIB. Albedo is predicted by SSIB over the land and is a function of solar zenith angle over the ocean. Monthly observed sea surface temperature (SST) from NOAA optimum interpolation (OI.v2) SST dataset (Reynolds et al. 2002) is used as boundary conditions. Climatological aerosol optical properties were specified as inputs to the scheme, as described in the previous section.

To validate the new radiation scheme, the data from the NASA World Climate Research Programme/Global Energy and Water-Cycle Experiment (WCRP/GEWEX) Surface Radiation Budget (SRB) Project[1] were used as the reference. The dataset used is the Release 2 of monthly shortwave radiative fields generated with the Pinker/Laszlo shortwave algorithm (Pinker and Laszlo 1992), available from July 1983 to October 1995. Quality control is accomplished by comparisons with a number of sites of the Baseline Surface Radiation Network (BSRN) over a period of four years (1992-1995). Mean bias is found to be 0.9 W m^{-2} (estimate - observation), and the random error about ± 22.0 W m^{-2}. For analyzing the cloud radiative forcing, SRB longwave data are also used. The corresponding dataset is the Release 2.5 of monthly longwave radiative fields derived with the GEWEX LW algorithm (Fu et al. 1997). Comparisons with BSRN found the mean bias to be about -2.0 W m^{-2} (estimate - observation), and the random

---

[1]http://eosweb.larc.nasa.gov/PRODOCS/srb/table_srb.html

error about ± 13.3 W m^{-2}. The NCEP-NCAR reanalysis (hereafter NCEP-R: Kistler et al. 2001; Kalnay et al. 1996) is used as reference for comparing the model-simulated wind fields, temperature and humidity. For evaluation of the impact of the new solar radiation scheme on global precipitation, the data from the Global Precipitation Climatology Project (GPCP v2: Adler et al. 2003) established by the World Climate Research Program (WCRP), available from 1979 to present time were used.

4. Results

a. Global Energy Balance

The annual mean (1985-1994) global average solar radiation absorbed at top of the atmosphere (TOA), at the surface (SFC) and by the atmosphere (ATM) are shown in Table 1. The OPE and NEW model results appear in the first and fourth columns. The results from the N-WA runs (without aerosols and water vapor continuum) and from the N-A runs (without aerosols) are shown in the second and third columns, respectively. Fifth column shows satellite-derived observations from the SRB datasets. The sixth column shows the mean and standard deviation from all models participating in AMIP (Wild 2005; Wild et al. 2006).

As compared with the operational model integration, the atmospheric absorption increases by 5 W/m^2 while the absorption at the surface decreases by 8 W/m^2 in the new model integration. The net effect is a reduction of 3 W/m^2 in the net shortwave absorbed by the Earth, bringing the model's result in agreement with observations. The largest change in atmospheric absorption (4 W/m^2) is between N-A and NEW, showing that accounting for scattering and absorption of background aerosols is more important than for water vapor continuum absorption

11

or the gaseous absorption. However, the clear-sky absorption values over ocean and land (see Table 2) indicate that the difference between the model results and satellite-derived estimates are probably related to the simple aerosol climatology used in the study. The aerosol loading seems to be overestimated over oceans and underestimated over land.

Disregarding the effects of clouds, N-WA, N-A and NEW atmospheres absorb 2 W/m^2, 6 W/m^2 and 10 W/m^2 more than the OPE model atmosphere. At the same time, the radiation absorbed at the surface is lower by -4 W/m^2, -7 W/m^2 and -17 W/m^2, respectively. The differences between the clear-sky and all-sky results show an underestimation of clouds' contribution to atmospheric absorption. In fact, the model has less atmospheric absorption in cloudy-sky than in clear-sky conditions, while the satellite derived results show the opposite effect. Results shown in Table 2 demonstrate that this happens over ocean and land, and for both OPE and NEW models. Over the oceans, there is a +4 W/m^2 bias in clear-sky atmospheric absorption and a -5 W/m^2 bias in cloudy-sky absorption. Over land, the bias in clear-sky and cloudy-sky are -3 W/m^2 and -8 W/m^2 respectively.

However, despite the model's deficiencies in the cloud parameterization, the changes in the shortwave scheme improve the average shortwave cloud radiative forcing (CRF). Moreover, Tables 1 and 2 clearly show that the NEW model fluxes are more accurate than OPE model fluxes, for both clear-sky and all-sky conditions. This is due to the use of updated water vapor absorption parameterization and the inclusion of absorption by weak water vapor lines, water vapor continuum, O_2, CO_2, and aerosols.

b. Heating and Temperature

Fig. 1 shows the zonal mean atmospheric absorption for the OPE, N-WA, N-A and NEW model results as well as the satellite-derived observations. The differences between the model results and observations are more pronounced in the summer hemisphere. From the clear-sky results shown in Figs. 1a and 1b, one can see that the main impact comes from considering the scattering and absorption of background aerosols, particularly south of 60^oS during DJF and between $5–45^oN$ during JJA. The absorption due to the water vapor continuum is the second most important contribution, mainly over the equatorial, tropical and subtropical regions. The changes in the gaseous absorption is the least important factor and its impact increases poleward of the summer hemisphere.

The all-sky atmospheric absorption is presented in Figs. 1c and 1d. Once can see that the model does not accurately accounts for the clouds' effects on atmospheric absorption in the equatorial and summer tropical regions. Yet, the model results are substantially improved in the integration with the NEW model. The only exception is the region around 60°. Moreover, the agreement between the model results and observations poleward of 15° of the winter hemisphere is within $1–2\,\mathrm{W\,m^{-2}}$ in this case.

Fig. 2 shows the impact of the extra atmospheric absorption in the vertical heating of the atmosphere. Note that below 750hPa there is a systematic increase in the heating rates. The difference between the NEW and OPE models grows northward of 60^oS. It is 0–15% between $60–40^oS$, 15–30% between $40^oS–20^oN$ and 30–60% between north of 20^oN. The high values of the heating rate difference from the surface to 750 hPa are related to solar radiation absorption by the background aerosols located in the near-surface layer (new solar radiation scheme). The systematic increase of this difference northwards is due to the large impact of the absorption

by the continental aerosols included over the land points in the NEW model. Note, that the oceanic aerosol type included over the ocean points is characterized by weak absorption of solar radiation. There is also a general increase of heating rates above 300hPa, which is related to the 10–40% increase of specific humidity in this region (figure not shown) and to an enhanced ozone absorption in the NEW Model (which is based on HITRAN96). However, the largest increase is found over Antarctica and some cooling is found in the middle troposphere, between 300–600hPa.

The differences between model and NCEP-R temperatures are shown in Figs. 3a and 3b. The OPE model shows a cooling bias all year round in the troposphere south of 40°S and in the upper troposphere north of 40°N. However, Figs. 3c and 3d show a general warming of the atmosphere with the NEW model with the highest temperature increases in the summer polar troposphere (up to 3 K warmer around 200 hPa) and in the stratosphere (up to 5 K warmer). A temperature decrease by less than 1K is observed in some regions up to 300hPa. This happens over the tropics and near the North Pole during DJF, and north of 40°S during JJA. Thus, the *CLIRAD-SW-M* scheme helped to decrease the OPE model temperature bias. Further more, the higher temperature in the upper troposphere increases its static stability and will certainly lead to changes in the atmospheric circulation.

c. Atmospheric Circulation

Figs. 4a and 4b show the zonal mean of the zonal wind for the NEW model. General characteristics such as the upper-level subtropical jets and tropical easterly winds are well captured. However, as noticed by Cavalcanti et al. (2002) (see Fig.2 therein), the jet intensity in the CPTEC/COLA model is too high. Figs. 4c and 4d show the differences between the NEW

and OPE model mean zonal winds. Both northern and southern hemisphere jets are weakened, more significantly during DJF. This weakening comes from the warming produced near the poles, shown in Fig. 3, and the consequent reduction of the meridional temperature gradient (Souza et al. 1997). During DJF, tropical easterlies are weakened, reducing model bias, due to the cooling in the middle troposphere equatorial region, shown in Fig. 3.

The zonal mean vertical circulation is shown in Fig. 5. During DJF, the upward branch of the Hadley cell is located at approximately 15^oS and 5^oN, as in the NCEP reanalysis, but the intensity is overestimated below 600hPa. These latitudes correspond to the more convective areas during this time of the year, such as the Indian Ocean, northern part of the South Pacific Convergence Zone (SPCZ), the north-west part of the South Atlantic Convergence Zone (SACZ) and the Intertropical Convergence Zones (ITCZ), where the KUO convection scheme is known to produce excessive precipitation. During DJF, the Ferrel cells are stronger in the model than in the reanalysis, mainly in the southern hemisphere. During JJA, the ascent branch of the Hadley cell is positioned around 10^oN, slightly more intense than the reanalysis, but the subsidence branch is well described.

The NEW model has a weaker meridional circulation, but this is more evident in the Hadley cell and in the southern polar cell, both during DJF and JJA. Some weakening is also found in the Ferrel cell in the Southern Hemisphere. The reduction of the meridional flow intensity is due to the increase of the atmospheric stability observed in Fig. 3, and allows for a reduction in the moist convective forcing. These changes related to the extra atmospheric absorption of the NEW model helped bringing the model closer to observations.

d. Surface Fluxes

The biases in clear-sky solar radiation surface fluxes simulated by the NEW and OPE models are shown in Fig. 6, as differences between model results and SRB estimates. The biases over continents are substantially reduced from 40–60 W m^{-2} to 10–20 W m^{-2}. Over the oceans, however, the biases change from +12 W m^{-2} to -7 W m^{-2} (see also Table 1). This indicates that climatological value of aerosol loading considered over the ocean (continent) is too high (low) when compared with the values used for deriving the SRB clear-sky fluxes.

Fig. 7a shows the difference between the NEW model and observations in the all-sky flux at the surface. Comparisons with the results from the OPE model (not shown) show that the bias is reduced, while the spatial distribution of the differences remain the same. There is a high spatial correlation between these differences and the differences in cloud cover fraction, as can be seen comparing Figs. 7a and 7b. Notice, for instance, the region of the Atlantic Ocean close to the eastern coast of Brazil, the SPCZ region, or the southern hemisphere midlatitudes.

The difference between the OPE model and NCEP-R sensible heat fluxes at the surface is shown in Fig. 8a. Notice that the largest biases are seen over continental regions, particularly, over South and North America. Fig. 8b shows that the NEW model reduces the bias and produces a general decrease of the sensible heat transfer at the surface and therefore is likely to decrease boundary layer turbulence. The reduction over the oceans, which have a prescribed surface temperature, must come from the less intense low level circulation alone (see Figs. 4a and 4c). The reduction over the continental regions, however, stems also from the large reduction of the solar radiation incident at the surface.

Fig. 9a shows the difference in the latent heat flux at the surface between the OPE model and NCEP-R. The largest differences are found where deep convection develops. For instance,

16

over the SPCZ, the Atlantic ITCZ and the NH storm tracks the difference reaches 80 W m^{-2}.

Fig. 9b shows that there is a decrease of the latent heat flux exactly over these regions, except

for the Atlantic ITCZ and South America. However, the spatial distribution of the differences

was not changed with the new model (figure not shown).

e. Cloud Radiative Forcing

It is important to notice that errors in cloud optical depth and/or cloud top-altitudes can

also contribute to the errors in the all-sky flux at the surface. To further investigate this issue,

we analyzed the cloud radiative forcing (CRF) in the same way as made by Potter and Cess

(2004). The SW and LW cloud radiative forcing (Ramanathan et al. 1989; Harrison et al. 1990)

are defined as the difference between the clear-sky and all-sky outgoing fluxes at the top of the

atmosphere:

$$SWCRF \quad = \quad SWF_{TOA}^{\uparrow c} - SWF_{TOA}^{\uparrow} \qquad (1)$$

$$LWCRF \quad = \quad LWF_{TOA}^{\uparrow c} - LWF_{TOA}^{\uparrow} \qquad (2)$$

Then the net cloud radiative forcing (netCRF) is given by $netCRF = SWCRF + LWCRF$

and for regions where there is a balance between SWCRF and LWCRF, $netCRF \sim 0$ and the

ratio $N = -SWCRF/LWCRF \sim 1$. In Fig. 10a we show the observed netCRF. The differ-

ence between the NEW model and SRB netCRF is shown in Fig. 10b. There is no significant

improvement from the OPE model results (analysis not shown). This was expected since both

versions of the CPTEC AGCM use the same longwave, cloud and convection parameterizations

(see section 2).

For a detailed analysis of the radiative forcing, the region marked in Fig. 10b was chosen,

17

where the model shows a reasonable agreement with the observed netCRF. This region in the tropical western Pacific (10°N to 5°S and 117.5°E to 170°E) is dominated by deep convection and therefore netCRF∼0 and N∼1 (Potter and Cess 2004). Fig. 11 presents a scatter plot of N x netCRF for the average SRB netCRF shown in Fig. 10 and the simulations with the NEW model. Each point on the plot corresponds to a grid box within the selected region. Because this plot is based on the average DJF distributions of SW and LW cloud radiative forcing, the points represent time averages of cloud systems and not specific cloud systems.

In this region, the NEW model produces overly bright clouds (spread in the upper left corner) and little thin cirrus (lower right). The area average results in a negative netCRF bias of -11 W m^{-2}. The failure to simulate the observed CRF at TOA and all-sky shortwave at the surface is a consequence of errors in the vertical and spatial distributions of cloud cover and cloud optical depth. Moreover, these errors are intrinsically related to the model deficiencies in the convection parameterization because tropical convergence depends on the energy fluxes into the atmospheric column (Neelin and Held 1987). Fig. 12 shows a scatter plot of convective precipitation versus SWCRF over the deep convective regions in the tropical oceans (annual mean SST>27°C and 20°S–20°N). Observed and model-simulated SWCRF decrease roughly linearly with increasing precipitation, but data seem to be offset. A closer look reveals that the model fails to produce low convective rainfall (<2 mm day^{-1}) and overestimates high convective rainfall (>10 mm day^{-1}). In fact, since SWCRF is overestimated and LWCRF agrees well with observations (not shown) the netCRF (which should not vary with precipitation) decreases with increasing precipitation by 7 W m^{-2}/mm day^{-1}. This means the model is holding less radiative energy as convection increases.

f. Precipitation

As mentioned by Cavalcanti et al. (2002), the model overestimates the precipitation over parts of South America, South Pacific and Intertropical Convergence Zones. However, with the improvement in the shortwave radiation scheme some of the systematic errors were diminished. Fig. 13 shows, for each model run, the difference in the global mean precipitation to the OPE model ensemble mean. Notice that the average reduction in precipitation is statistically significant, even though the absolute value of $0.08 \, \mathrm{mm \, day^{-1}}$ (3%) is small when compared to the total precipitation.

These changes in precipitation have a large spatial variation and most of the reduction is found over the oceans, as shown in Fig. 14. Comparing with the results of Cavalcanti et al. (2002), we see that the new radiation scheme helped to reduce the model bias over the SPCZ region by 0.5–$1.0 \, \mathrm{mm \, day^{-1}}$ and over the northern hemisphere storm tracks region, by $0.5 \, \mathrm{mm \, day^{-1}}$. Over South America, there was a reduction of 0.5–$1 \, \mathrm{mm \, day^{-1}}$ of the model systematic error over some regions. However, these figures are smoothed by the 10-yr time average. The changes in precipitation during each individual DJF period are larger by a factor ~ 5 approximately, as shown in Fig. 15. Over the SACZ region, for instance, differences of ± 2–$3 \, \mathrm{mm \, day^{-1}}$ (15–25%) are found every year.

5. Discussion

As compared with the OPE model results, the N-WA, N-A and NEW model show an increase in atmospheric absorption (Table 1) of 0.1%, 1.5% and 7.9% for all-sky conditions, and 1.5%, 7.9% and 14% for clear-sky conditions, respectively. These values show that the most

important changes introduced with the NEW model are related first to the scattering and absorption by climatological aerosols and second to the absorption by water vapor continuum. The satellite-derived data used as reference, when compared to ground truth, has a mean bias about 0.9 W m^{-2} and a random error about $\pm$22.0 W m^{-2}. This means that the remaining +2W m^{-2} bias in the clear-sky atmospheric absorption with the NEW model is within the precision of SRB satellite estimates. We should notice that the current version of *CLIRAD-SW-M* is based on the HITRAN-96 molecular absorption database and uses the CKD-2.1 version of the water vapor continuum of Clough et al. (1989). The impact of different spectroscopic databases and versions of water vapor continuum on the calculated solar radiative fluxes is discussed by Fomin et al. (2004). A flux difference of 1-3 W m^{-2} is found due to the change of the HITRAN-96 database with the CKD-2.1 continuum to the HITRAN-2001 database with the CKD-2.4 continuum in the line-by-line calculations. This flux difference which is mainly related to the change of the continuum version can affect the model results. Moreover, Fig. 6 shows a clear difference between the remaining bias in the surface flux over continents and oceans, which indicates that climatological values of aerosol loading considered over the ocean (continent) was too high (low) when compared with the values uses for deriving the SRB clear-sky fluxes.

Fig. 7 shows the largest impact of the new scheme on the surface shortwave fluxes to be exactly over the regions where the largest model bias were found. There are still large differences from observations in the all-sky surface flux (from -40 to +60 W m^{-2} in the tropical and subtropical regions) which we show to be related to the deficiencies in the model cloud parameterization (compare Figs. 10b and 7a). The cloud radiative forcing analysis shows similar deficiencies in both OPE and NEW models, which was expected as both use the same longwave and cloud parameterizations. Over the Pacific ITCZ, the OPE and NEW CPTEC models, like

the original COLA model (Fig. 6 from Potter and Cess 2004) produces overly bright clouds and little thin cirrus, which results in a negative bias in the shortwave flux at the surface. It is interesting to compare the results from Potter and Cess (2004) obtained for the COLA model with our result with the NEW model, as both rely on the same cloud parameterization. Fig. 11 in the previous section and Figs. 6 and 7 from Potter and Cess (2004) show that improvements implemented at CPTEC led to a significant improvement in the model CRF.

The extra radiative heating of the atmosphere (Fig. 2) led to significant changes in the temperatures of the polar summer troposphere (Fig. 3). However, the increase in the temperature which was of the order of 3K, is not enough to correct the OPE model bias of about -10K. In the stratosphere the changes were around 4K and over the winter pole, more than 8K. These results agree with previous results of Ramanathan et al. (1983) and Hart et al. (1990) who showed the equilibrium between radiative and dynamic forcings in the stratosphere to be very sensitive to the parameterization of radiation. However, even with this increase in the stratospheric temperatures due to the extra atmospheric absorption of solar radiation, there is still a -10K bias. Results from Ramanathan et al. (1983) indicate that this might be related to the longwave scheme. Ramanathan et al. (1983) estimated that if the scheme they used assumed a constant water vapor mixing ratio of 3ppm in the stratosphere (as in NEW and OPE models), their simulations would have overestimated the cooling rates by about 0.1K/day and cooled the stratosphere by 10K.

With the reduced availability of energy at the surface, the sensible heat over the continents and latent heat over the oceans were reduced, as shown in Figs. 8 and 9. This means a reduction of energy available for convection, which is in accordance with the weakening of the meridional circulation (Fig. 5) and the reduction of precipitation (Fig. 13). This is similar to the results of Morcrette (1990) for short-term integrations of the ECMWF model. He showed

that a decrease in the bias of atmospheric absorption of solar radiation from +15~20% to less than +5% led to a 15% stronger hydrological cycle and meridional circulation. In our study, the improved solar radiation scheme helped to reduce the negative bias from -15% to -7% (see Table 1) and slowed down the hydrological cycle by 3% on average. Considering South America only, the OPE model bias was reduced from +43 $\mathrm{W\,m^{-2}}$ to +23 $\mathrm{W\,m^{-2}}$ in the NEW model. The reduction of the precipitation over the ocean in the SACZ region was only -1 $\mathrm{mm\,day^{-1}}$ (~6%). However, these figures are smoothed by the 10-yr time average. When we analyze individually each DJF period, we find positive and negative differences of $\pm$2–3 $\mathrm{mm\,day^{-1}}$ (15–25%) which are slightly unbalanced. Our results indicate that significant impacts on the hydrological cycle are to be expected at monthly time scales but not at yearly time scales. This might be important for seasonal forecasting of temperature and precipitation anomalies, particularly when anomalies are calculated by differences between an ensemble of short forecast integrations and a multi-year model climatology. One should expect, however, that the convection and surface parameterizations play an important role in determining the response of the hydrological cycle to changes in the radiation. In fact, preliminary results with the NEW model and the GRELL deep convection scheme (Figueroa et al. 2006) have shown a larger response of the hydrological cycle in the decadal time scale and a great improvement in the model DJF precipitation spatial distribution.

6. Summary

We have shown that using the *CLIRAD-SW-M* scheme the CPTEC GCM simulates fluxes and atmospheric absorption closer to observations than those provided by the operational model.

The global yearly average underestimation of atmospheric absorption decreased from $-9\ W/m^2$ to $-6\ W/m^2$, while overestimation of solar radiation at the surface decreased from +14 W/m^2 to +6 W/m^2. Comparisons with model runs without the background aerosols included in the radiation scheme showed that they are responsible for approximately 80% of this extra absorption, even thou they respond only to 50% of the clear-sky extra absorption. Moreover, we have also shown that the agreement between the model and observations under these conditions is now within ± 3 W/m^2 which is well within the precision of the observed data.

The zonal average of the model atmospheric absorption has shown significant improvements in the model integrations with the *CLIRAD-SW-M* scheme. For both DJF and JJA, the biases over the winter hemisphere were completely corrected while over the summer hemisphere they were reduced to less than -15 W/m^2, with a large impact of the aerosol scattering and absorption near the poles and of the water vapor continuum absorption in the equatorial and tropical regions. The largest improvement was over Antarctica, where the bias was reduced from -45 W/m^2 to -12 W/m^2 during DJF. However, we found that there is still bias in surface fluxes mainly due to model deficiencies related to cloud parameterization.

The extra atmospheric heating increased the tropospheric temperatures by $\sim$3K and the stratospheric temperatures by $\sim$5K. In the polar night region, due to dynamic forcing, temperature changes of $\sim$8K were found, which reduced the model temperature bias. These results agree with previous results of Ramanathan et al. (1983) and Hart et al. (1990) who showed that the equilibrium between radiative and dynamic forcings in the stratosphere is very sensitive to the parameterization of radiation. However, there is still a cold bias of -10K in the polar stratosphere, which probably comes from the use of a constant 3ppm water vapor mixing ratio in this region (Ramanathan et al. 1983).

The increase in temperature in the upper troposphere and reduction of the temperature gradient between the poles and the equatorial region increased the static stability and reduced both the meridional and zonal circulations. The intensity of the tropospheric jets is reduced by 7–8%, while that of the polar night stratospheric jet were increased by 5-10%. The vertical velocities in the Hadley and southern polar cells were reduced by 20% ($\sim$0.005 Pa/s). Both results bring the model simulated wind fields closer to observed values.

It was also shown that the reduced availability of latent energy for the saturated convective processes weakened the meridional circulation and slightly slowed down the hydrological cycle. The overestimation of the global yearly average of precipitation decreased from +0.8 mm day^{-1} to +0.7 mm day^{-1}. The new radiation scheme helped to reduce the model bias over the SPCZ region by 0.5–1.0 mm day^{-1} and over the northern hemisphere storm tracks region, by 0.5 mm day^{-1}. In the monthly time scale the impacts are stronger. Over the SACZ region we found positive and negative differences of $\pm$2–3 mm day^{-1} (15–25%) during individual DJF periods.

This is potentially important for seasonal forecasting particularly when anomalies are calculated by differences between an ensemble of short forecast integrations and a multi-year model climatology, as operationally performed by CPTEC. However, further investigation of this subject is necessary and will be done in a future study. Moreover, the convection and surface parameterizations probably play a more important role in determining the magnitude of the response of the hydrological cycle. In fact, preliminary results from Figueroa et al. (2006) with the NEW model and the GRELL deep convection scheme have shown a larger response of the hydrological cycle and a great improvement in the model precipitation.

We stress that the use of GCMs in operational seasonal forecasting or in climate change

assessments requires that the model simulates well the present observed climate and its variability. In this sense, this study shows how a new shortwave radiation parameterization allowed for significant improvements in the CPTEC model ability to represent observed characteristic features of the earth radiation budget, atmospheric circulation and precipitation.

References

Adler, R. F. et al., 2003: The version 2 Global Precipitation Climatology Project (GPCP) monthly precipitation analysis (1979-present). *J. Hydrometeor.*, **4**, 1147–1167.

Anthes, R. A., 1977: Hurricane model experiments with a new cumulus parameterization scheme. *Mon. Weath. Rev.*, **105**, 270–286.

Briegleb, B. P., 1992: Delta-eddington approximation for solar radiation in the NCAR Community Climate Model. *J. Geophys. Res.*, **97**, 7603–7612.

Cavalcanti, I. F. A. et al., 2002: Climatological features in a simulation using CPTEC-COLA AGCM. *J. Climate*, **15**, 2965–2988.

Cess, R. D. et al., 1995: Absorption of solar radiation by clouds: Observations versus models. *Science*, **267**, 496–499.

Chagas, J. C. S., P. Nobre, and M. Malagutti, 2004: Modifications on the CPTEC global model radiation scheme. *Proceedings of XIII Brazilian Meteorology Conference*, Fortaleza-CE.

Chou, M. D. and M. J. Suarez, 1999: A solar radiation parameterization (CLIRAD-SW) for atmospheric studies. Tech. Rep. Series on Global Modeling and Data Assimilation, **15**, NASA, TM-1999-104606, 40 pp.

Clough, S. A., F. X. Kneizys, and R. W. Davies, 1989: Line shape and the water vapor continuum. *Atmos. Res.*, **23**, 299–241.

Clough, S. A. et al., 2005: Atmospheric radiative transfer modeling: A summary of AER codes. *J. Quant. Spec. Rad. Trans.*, **91**, 233–244.

Collins, W. D., 2006: *Frontiers of Climate Modeling*, chap. Unresolved Issues in Atmospheric Solar Absorption. Cambridge University Press.

Collins, W. D., J. M. Lee-Taylor, D. P. Edwards, and G. L. Francis, 2006: Effects of increased near-infrared absorption by water vapor on the climate system. *J. Geophys. Res.*, **111**, D18 109.

Cusack, S., A. Slingo, J. M. Edwards, and M. Wild, 1998: The radiative impact of a simple aerosol climatology on the Hadley Centre atmospheric GCM. *Quart. J. Roy. Meteor. Soc.*, **124**, 2517–2526.

Davies, R., 1982: *Documentation of the solar radiation parameterization in the GLAS Climate Model*. Goddard Space Flight Center.

Figueroa, S. N., T. Tarasova, H. M. J. Barbosa, J. P. Bonatti, and P. L. Silvia Dias, 2006: The impact of cumulus and radiation parameterization schemes on Southern Hemisphere summer climate simulated by CPTEC Atmospheric General Circulation Model. *Proceedings of 8 ICSHMO*, Foz do Iguaçu, Brazil, 1037–1040.

Fomin, B. and Y. Gershanov, 1996: Tables of the benchmark calculations of atmospheric fluxes for the ICRCCM test cases, part II: Short-wave results. Russian Research Center "Kurchatov Institute", Moscow, Russia, Vol. IAE-5990/1, 42pp.

Fomin, B., T. Udalova, and E. Zhitnitskii, 2004: Evolution of spectroscopic information over the last decade and its effect on line-by-line calculations for validation of radiation codes for climate models. *J. Quant. Spec. Rad. Trans.*, **86**, 73–85.

Fu, Q., K. N. Liou, and M. C. Cribb, 1997: Multiple scattering parameterization in thermal infrared radiative transfer. *J. Atmos. Sci.*, **54**, 2799–2812.

Gates, W., 1992: AMPI: The Atmospheric Model Intercomparison Project. *Bull. Amer. Meteor. Soc.*, **73**, 1962–1970.

Gates, W. et al., 1999: An overview of the results of the Atmospheric Model Intercomparison Project (AMIP). *Bull. Amer. Meteor. Soc.*, **80**, 29–55.

Harrison, E. F., P. Minnis, B. R. Barkstrom, V. Ramanathan, R. D. Cess, and G. G. Gibson, 1990: Seasonal variation of cloud radiative forcing derived from the Earth Radiation Budget Experiment. *J. Geophys. Res.*, **95**, 18 687–18 703.

Harshvardhan, D. and T. G. Corsetti, 1984: Longwave radiation parameterization for the UCLA/GLAS GCM. NASA Tech. Memo. 86072, 65P, Goddard Space Flight Center, Greenbelt, MD.

Harshvardhan, D., A. Randall, and T. G. Corsetti, 1987: A fast radiation parameterization for general circulation models. *J. Geophys. Res.*, **92**, 1009–1016.

Hart, T. L. et al., 1990: Atmospheric general circulation simulations with the BMRC Global Spectral Model: the impact of revised physical parameterizations. *J. Climate*, **3**, 436–459.

Hou, Y. T., 1990: Cloud-radiation dynamics interaction. Ph.D. thesis, University of Maryland, 209 pp.

Hurrell, J. W., J. J. Hack, B. A. Boville, D. L. Willianson, and J. T. Kiehl, 1998: The dynamical simulation of the NCAR Community Climate Model Version 3 (CCM3). *J. Climate*, **11**, 1207–1236.

Johns, T. C., R. E. Carnell, J. F. Crossley, J. M. Gregory, J. B. Mitchell, C. A. Senior, S. B. Tett, and R. A. Wood, 1997: The second Hadley Centre coupled ocean–atmosphere GCM: Model description, spinup and validation. *Climate Dyn.*, **13**, 103–134.

Kalnay, E. et al., 1996: The NCEP/NCAR 40-year Reanalysis Project. *Bull. Amer. Meteor. Soc.*, **77 (3)**.

Kiehl, J. T., 1994: Clouds and their effects on the climate system. *Phys. Today*, **47**, 36–42.

Kiehl, J. T., J. J. Hack, M. H. Zhang, and R. D. Cess, 1995: Sensitivity of a GCM climate to enhanced shortwave cloud absorption. *J. Climate*, **8**, 2200–2212.

Kistler, R. et al., 2001: The NCEP-NCAR 50 years reanalysis: Monthly means CD-ROM and documentation. *Bull. Amer. Meteor. Soc.*, **82**, 247–267.

Kuo, H. L., 1974: Further studies of the parameterization of the influence of cumulus convection on large-scale flow. *J. Atmos. Sci.*, **31**, 1232–1240.

Lacis, A. A. and J. E. Hansen, 1974: A parameterization for the absorption of solar radiation in the earth's atmosphere. *J. Atmos. Sci.*, **31**, 118–133.

Li, Z., L. Moreau, and A. Arking, 1999: On solar energy disposition: A perspective from observation and modeling. *Bull. Amer. Meteor. Soc.*, **78**, 53–70.

Lohmann, U. and R. Bennartz, 2002: Impact of improved near-infrared water vapor line data in simulations with the ECHAM4 general circulation model. *J. Geophys. Res.*, **107 (D16)**, 4288.

Mellor, G. L. and T. Yamada, 1982: Development of a turbulence closure model for geophysical fluid problems. *Rev. Geophys. Space Phys.*, **20**, 851–875.

Monin, A. S., 1986: *An introduction to the theory of climate*. D. Reidel, Dordrecht, Holland.

Morcrette, J.-J., 1990: Impact of changes to the radiation transfer parameterizations plus cloud optical properties in the ECMWF model. *Mon. Weath. Rev.*, **118**, 847–873.

Neelin, J. D. and I. M. Held, 1987: Modeling tropical convergence based on the moist static energy budget. *Mon. Weath. Rev.*, **115**, 3–12.

Pinker, R. and I. Laszlo, 1992: Modeling surface solar irradiance for satellite applications on a global scale. *J. Appl. Meteor.*, **31**, 194–211.

Plana-Fattori, A., E. P. Souza, and J. C. S. Chagas, 1997: Absorption of solar radiation by water vapor in the atmosphere. Part I: a comparison between selected parameterizations and reference results. *Brazilian J. Geophys.*, **15 (3)**, 275–290.

Pope, V. D., M. L. Gallani, P. R. Rowntree, and R. A. Stratton, 2000: The impact of new physical parameterizations in the Hadley Centre climate model: HadCM3. *Climate Dyn.*, **16**, 123–146.

Potter, G. L. and R. D. Cess, 2004: Testing the impact of clouds on the radiation budgets of 19 atmospheric general circulation models. *J. Geophys. Res.*, **109**, D02 106.

Ramanathan, V., R. D. Cess, E. F. Harrison, P. Minnis, B. R. Barkstrom, E. Ahmad, and D. Hartmann, 1989: Cloud-radiative forcing and climate: Results from the Earth Radiation Budget Experiment. *Science*, **243**, 57–63.

Ramanathan, V. et al., 1983: The response of a spectral general circulation model do refinements in radiative processes. *J. Atmos. Sci.*, **40**, 605–630.

Ramaswamy, V. and S. M. Freidenreich, 1992: A study of broadband parameterizations of the solar radiative interactions with water vapor and water drops. *J. Geophys. Res.*, **97**, 11 487–11 512.

Reynolds, R. W. et al., 2002: An improved in situ and satellite SST analysis for climate. *J. Climate*, **15**, 1609–1625.

Rothman, L. S. et al., 1983: AFGL trace gas compilation, 1982 version. *Appl. Opt.*, **22**, 1616–1627.

———, 1998: The HITRAN molecular database and HAWKS, 1996 edition. *J. Quant. Spec. Rad. Trans.*, **60**, 665–710.

———, 2003: The HITRAN molecular spectroscopic database: Edition of 2000 including 2001 updates. *J. Quant. Spec. Rad. Trans.*, **82**, 5–42.

Slingo, J. M., 1987: The development of verification of a cloud prediction scheme for the ECMWF model. *Quart. J. Roy. Meteor. Soc.*, **113**, 899–927.

Souza, E. P., P. L. da S. Dias, A. Plana-Fattori, and J. C. S. Chagas, 1997: Absorption of solar radiation by water vapor in the atmosphere. Part II: sensitivity tests with a general circulation model. *Brazilian J. Geophys.*, **15 (3)**, 291–306.

Tarasova, T., H. M. J. Barbosa, and S. N. Figueroa, 2006: Incorporation of new solar radiation scheme into CPTEC GCM. Tech. Rep. INPE-14052-NTE/371, Instituto Nacional de Pesquisas Espaciais.

Tarasova, T. and I. Cavalcanti, 2002: Monthly mean solar radiative fluxes and cloud forcing

over South America in the period of 1986-88: GCM results and satellite-derived data. *J. Appl. Meteor.*, **41**, 863–871.

Tarasova, T. and B. Fomin, 2000: Solar radiation absorption due to water vapor: Advanced broadband parameterizations. *J. Appl. Meteor.*, **39**, 1947–1951.

Tiedtke, M., 1984: The effect of penetrative cumulus convection on the large-scale flow in a general circulation model. *Contrib. Atmos. Phys.*, **57 (2)**, 216–239.

Wild, M., 2005: Solar radiation budgets in atmospheric model intercomparisons from a surface perspective. *Geophys. Res. Lett.*, **32**, L07 704.

Wild, M. and A. Ohmura, 1999: The role of clouds and cloud-free atmosphere in the problem of underestimated absorption of solar radiation in GCM atmosphere. *Phys. Chem. Earth*, **24B**, 261–268.

Wild, M., A. Ohmura, H. Gilgen, and E. Roeckner, 1995: Validation of general-circulation model radiative fluxes using surface observations. *J. Climate*, **8**, 1309–1324.

Wild, M. et al., 2006: Evaluation of clear-sky solar fluxes in GCMs participating in AMIP and IPCC-AR4 from a surface perspective. *J. Geophys. Res.*, **111**, D01 104.

Xue, Y., P. J. Sellers, J. L. Kinter III, and J. Shukla, 1991: A simplified biosphere model for global climate studies. *J. Climate*, **4**, 345–364.

Yamamoto, G., 1962: Direct absorption of solar radiation by atmospheric water vapor, carbon dioxide and molecular oxygen. *J. Atmos. Sci.*, **19**, 182–188.

Yu, H. et al., 2006: A review of measurement-based assessments of the aerosol direct radiative effect and forcing. *Atmos. Chem. Phys.*, **6**, 613–666.

List of Figures

FIG. 1. Zonal mean atmospheric absorption (W m^{-2}) averaged over (a) DJF and (b) JJA periods. Data from satellite derived observation (SRB, circle) and models OPE (thin line), N-WA (long dash), N-A (dot-dash) and NEW (thick line) are shown.
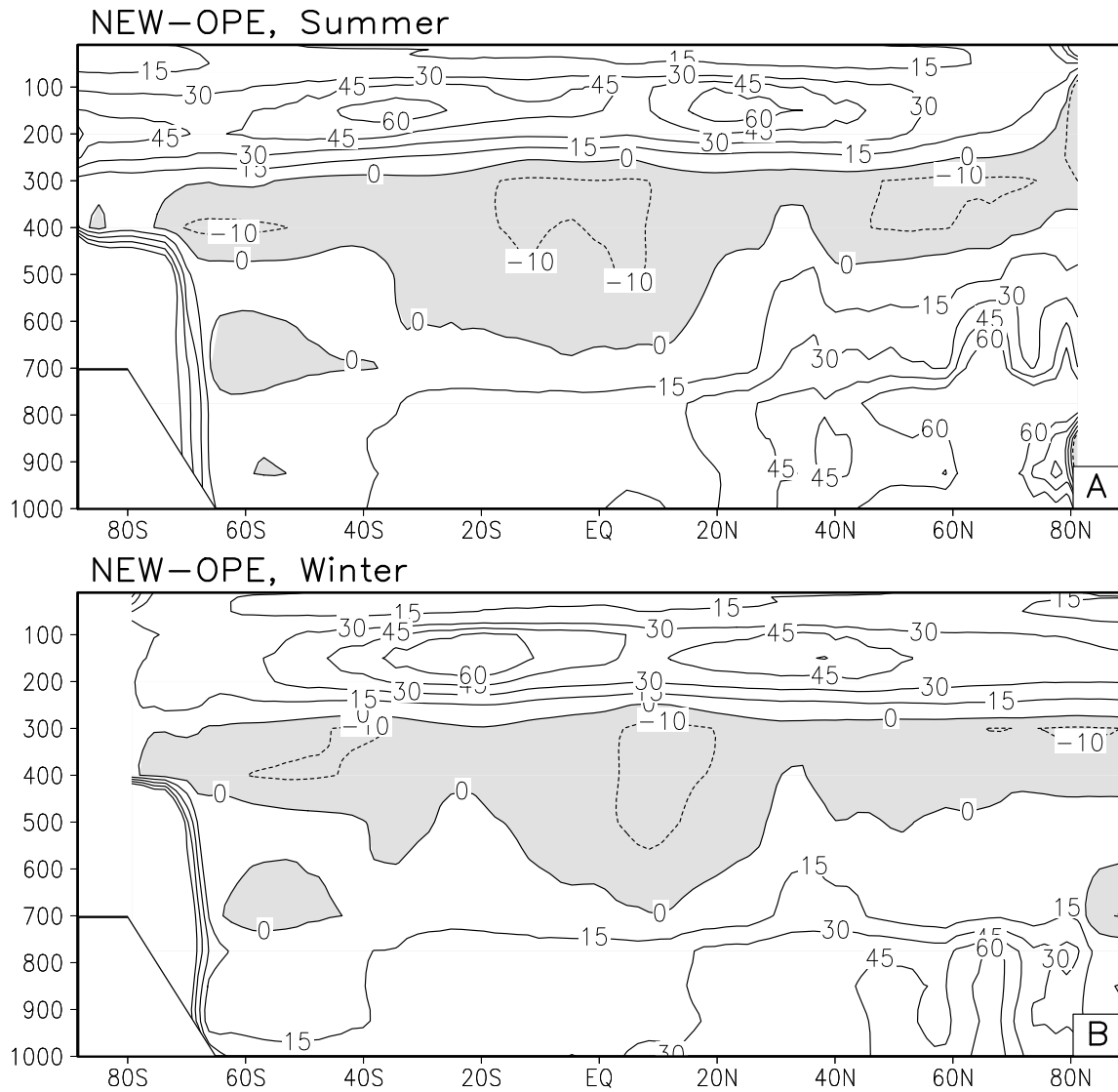
NEW—OPE, Summer

NEW—OPE, Winter

FIG. 2. Zonal mean shortwave heating rate difference (%) between NEW and OPE models during (a) DJF and (b) JJA periods. Negative values are shaded in gray.
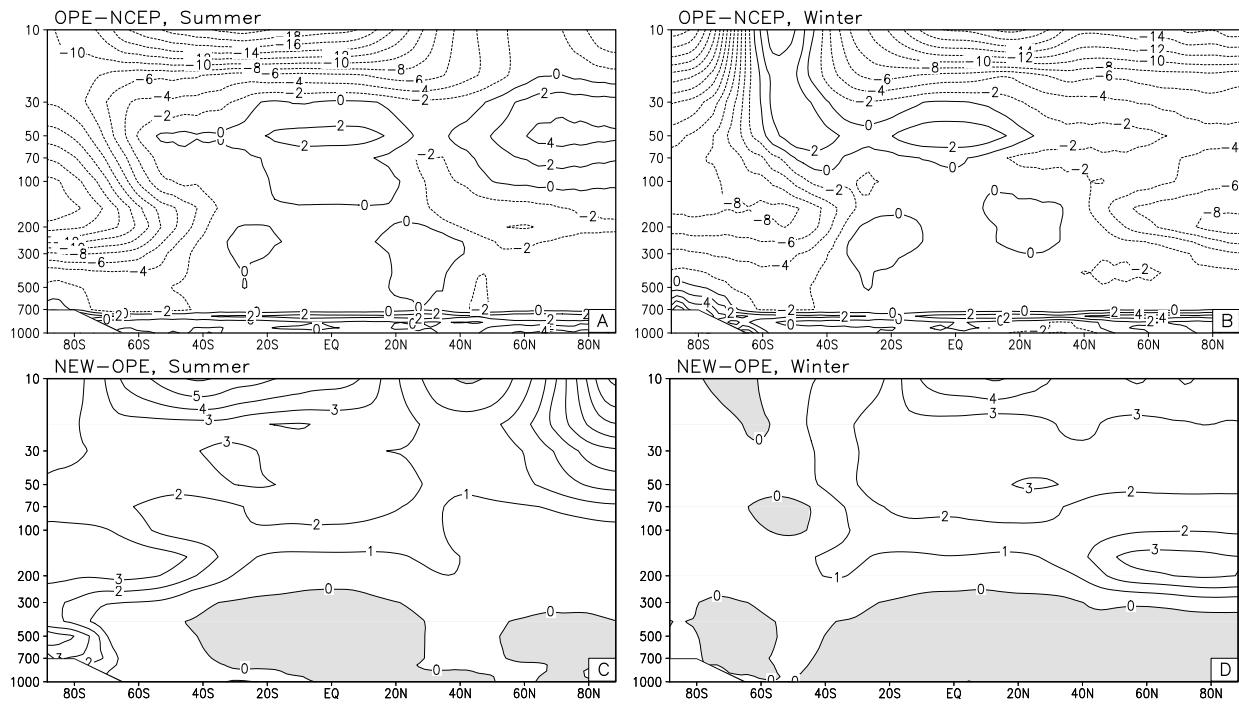
FIG. 3. Differences in zonal mean air temperature (^{o}C) between (a), (b) OPE model and NCEP reanalysis, and (c), (d) NEW and OPE models, during DJF (left) and JJA (right). Negative values are shaded in gray.
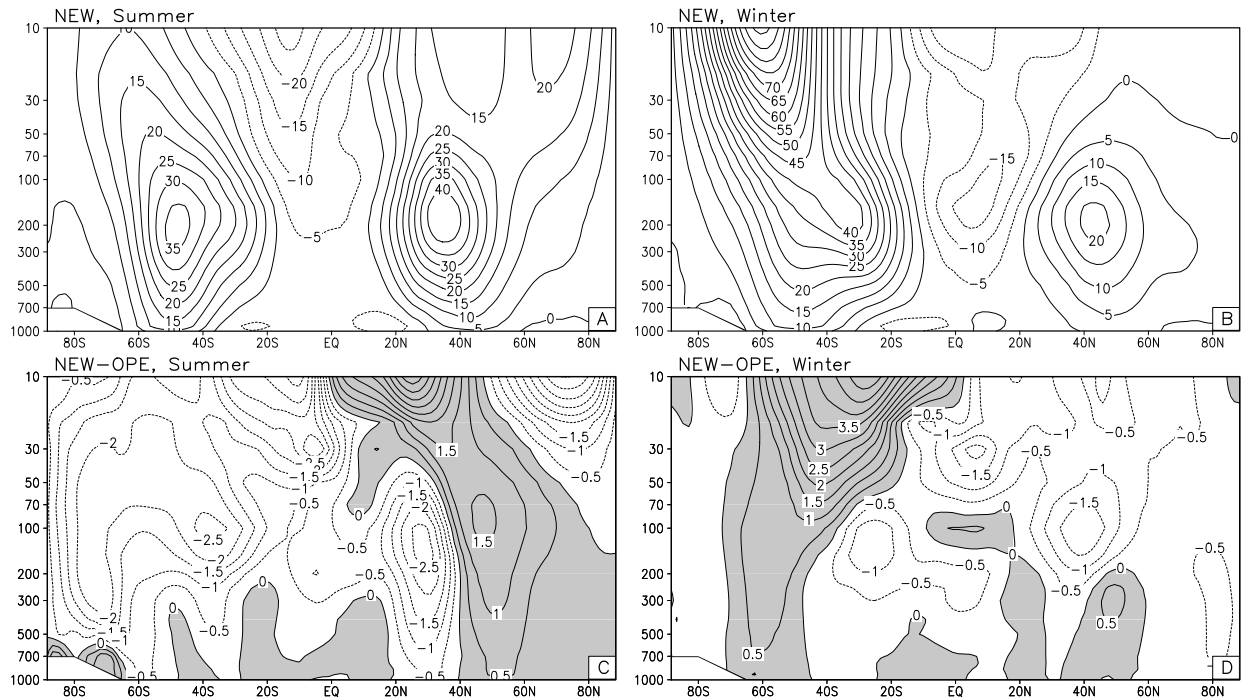
FIG. 4. Climatological vertical structure of zonal wind (m/s): NEW model (a) DJF and (b) JJA. The differences between NEW and OPE models are shown in (c) and (d) for DJF and JJA respectively, and positive values are shaded in gray.
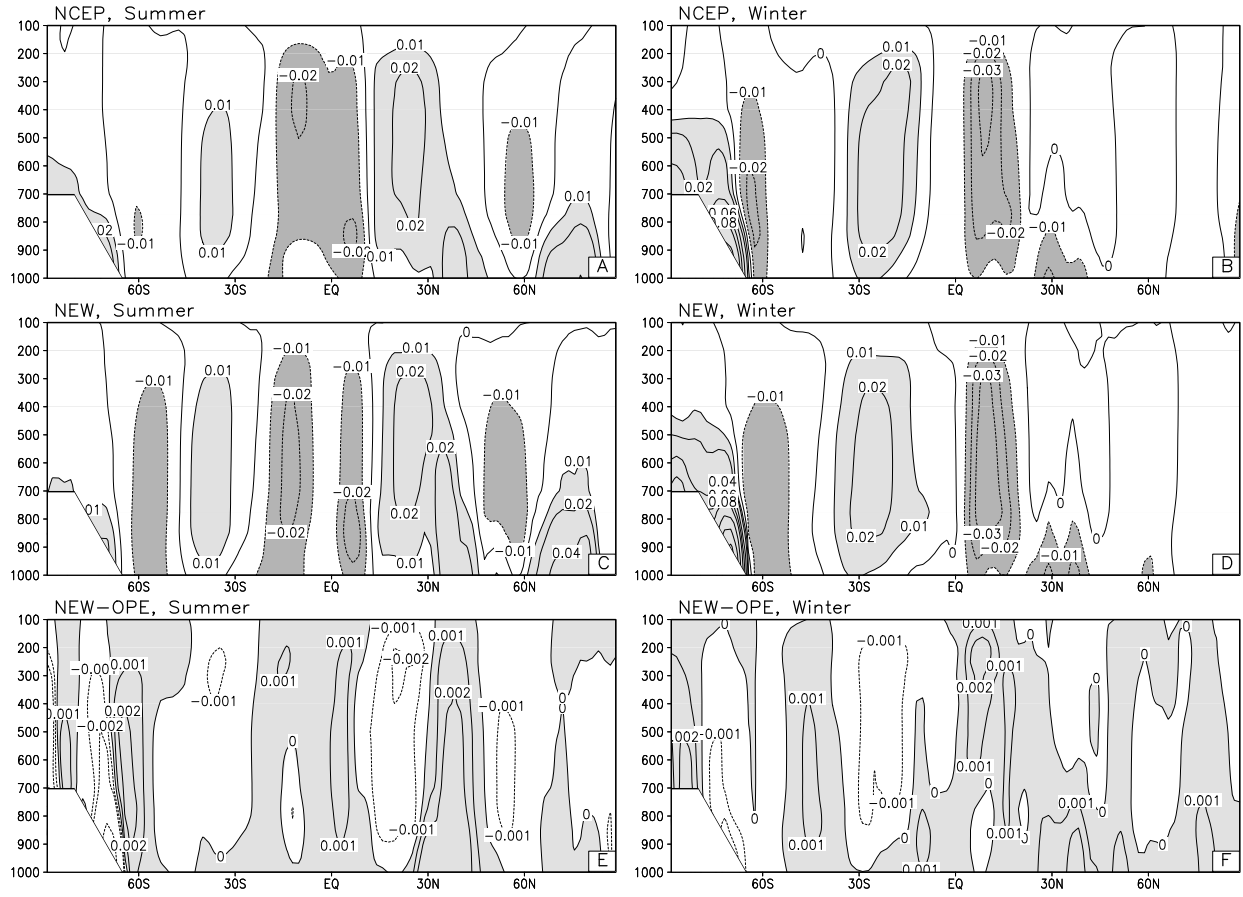
FIG. 5. Zonal mean vertical p-velocity (Pa/s): (a), (b) NCEP-R and (c), (d) NEW model, during DJF (left) and JJA (right) respectively. The difference between NEW and OPE are shown in (e) and (f), where positive p-velocity differences are shaded in gray.
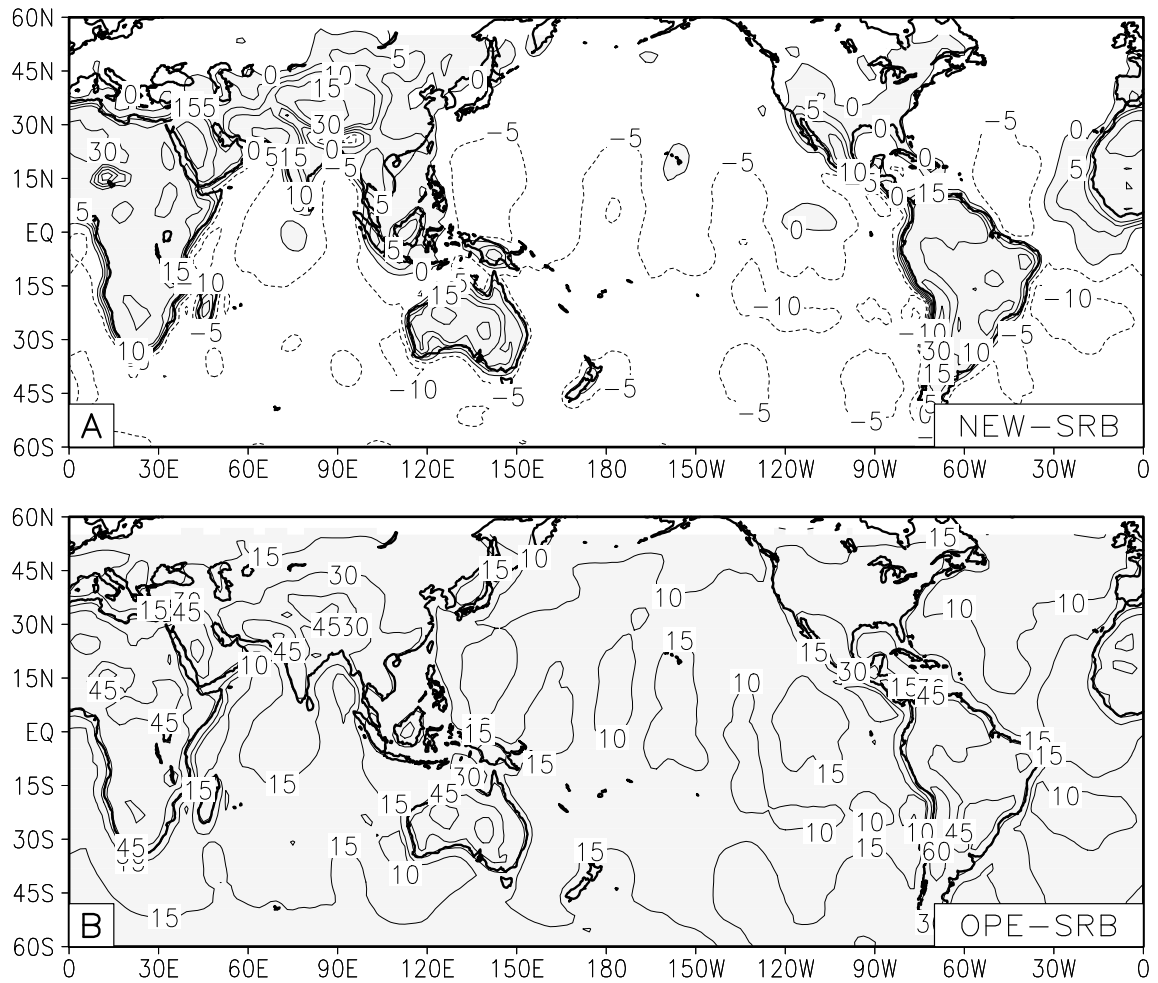
FIG. 6. Differences between (a) NEW and (b) OPE models and satellite-derived (SRB) estimations of DJF clear-sky shortwave radiation fluxes at the surface (W m^{-2}). Regions with a positive bias are shaded in gray.
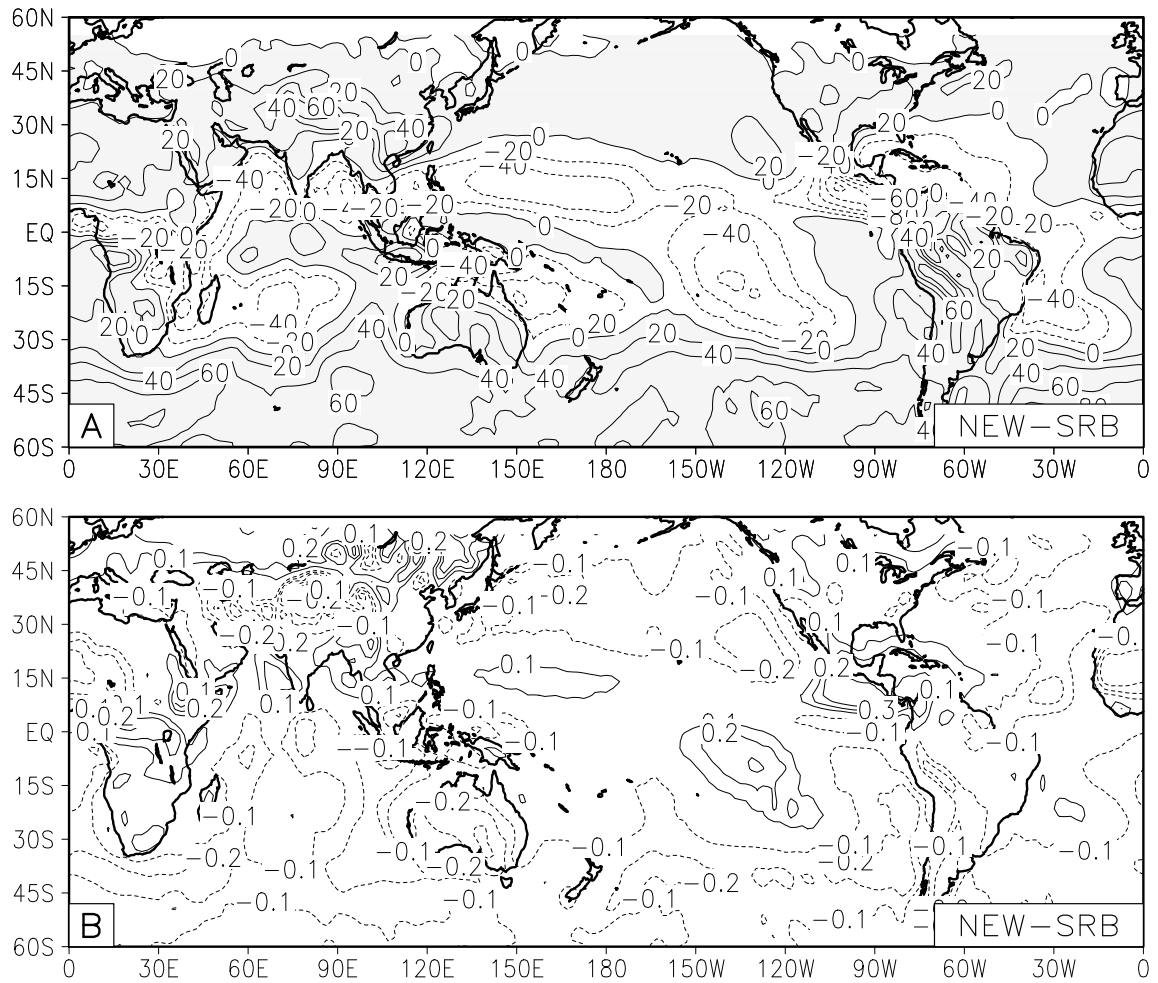
FIG. 7. Differences between NEW model and satellite-derived (SRB) estimations of (a) all-sky shortwave flux at the surface (W m^{-2}) and (b) total cloud cover during DJF. The spatial correlation coefficient between (a) and (b) is -0.66 and regions with a positive flux bias are shaded in gray.
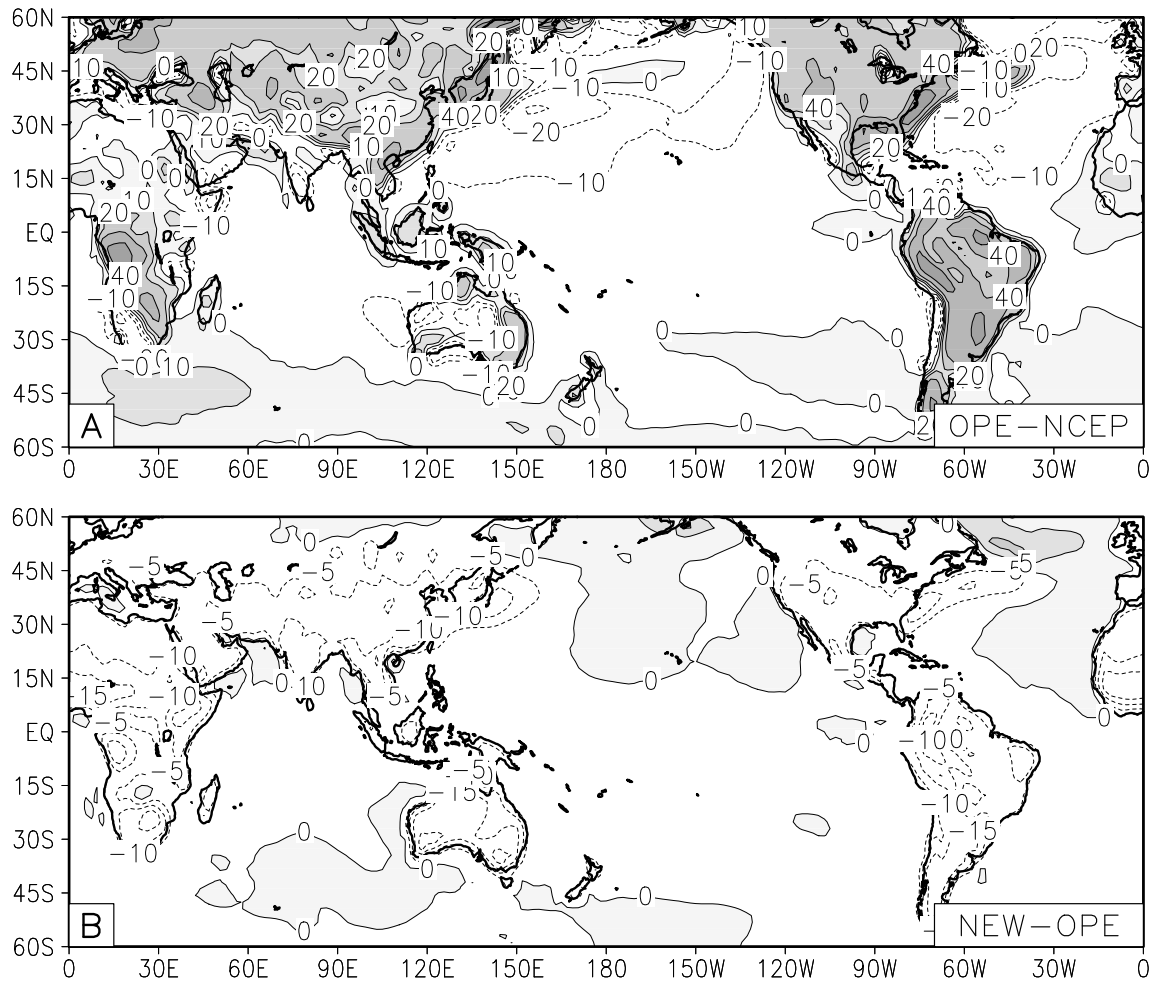
FIG. 8. Differences between (a) OPE and NCEP-R, and (b) NEW and OPE estimations of surface sensible heat flux (W m^{-2}), during DJF. Regions with a positive flux bias are shaded in gray.

43
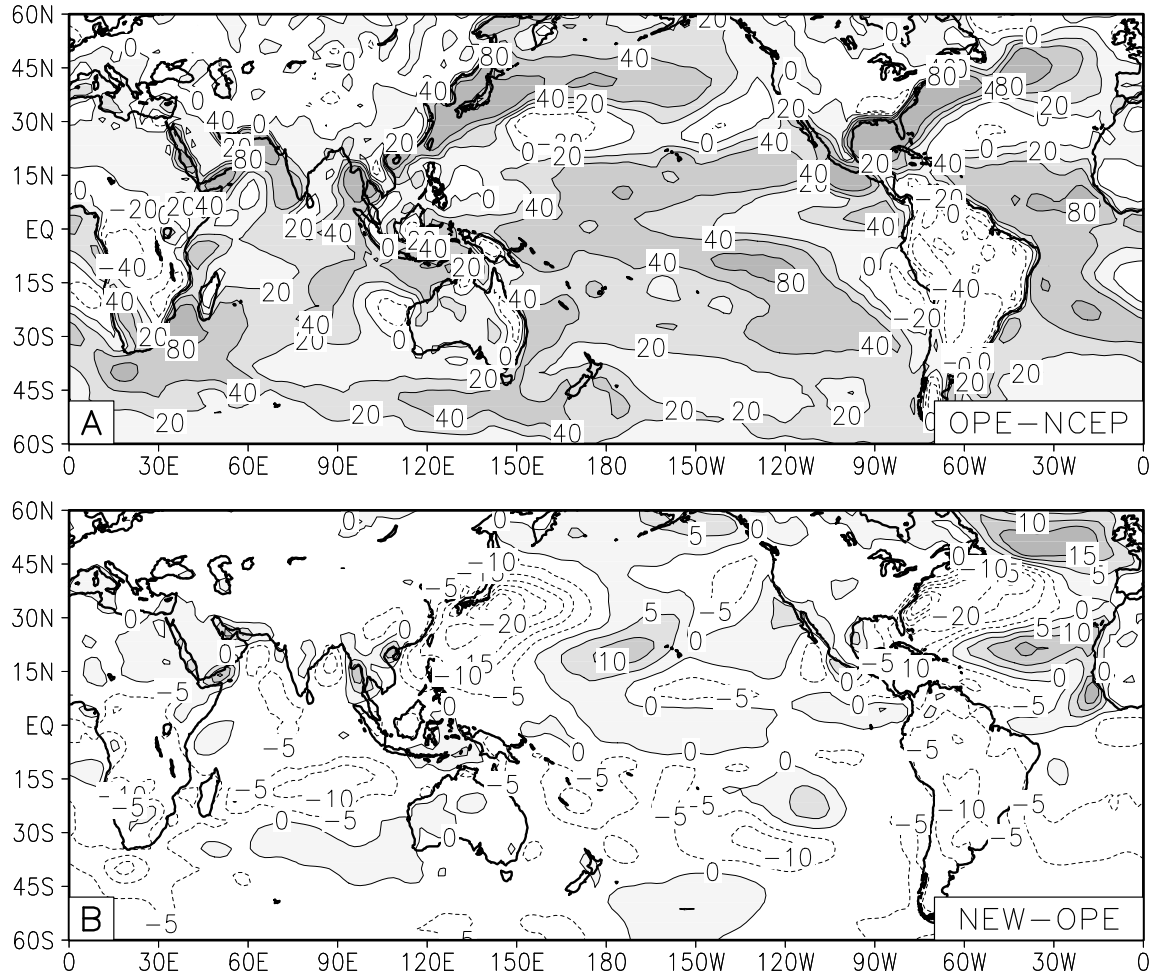
FIG. 9. Differences between (a) OPE and NCEP-R, and between (b) NEW and OPE estimations of surface latent heat flux (W m^{-2}), during DJF. Regions with a positive flux bias are shaded in gray.
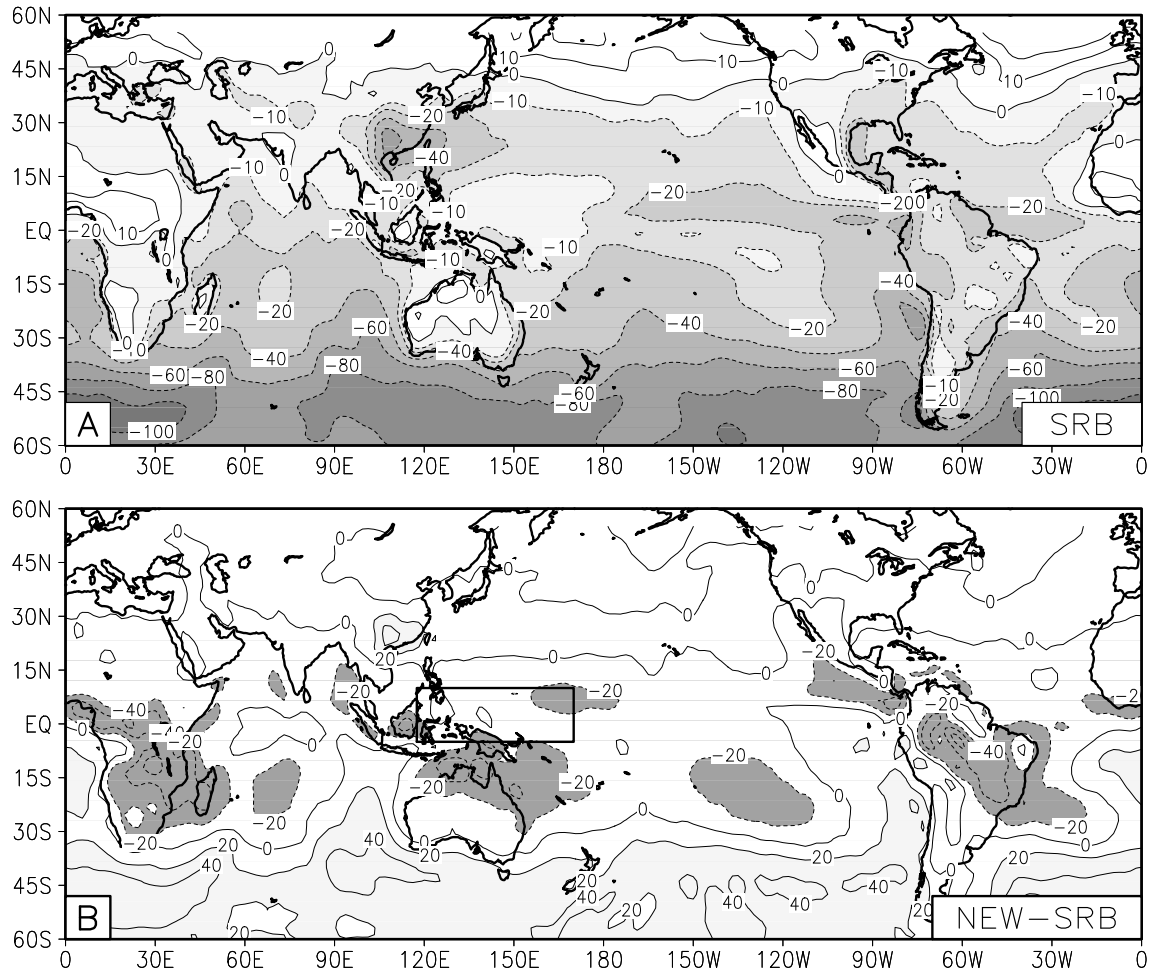
FIG. 10. Net cloud radiative forcing (W m^{-2}) from (a) satellite derived observations (SRB) and (b) differences between NEW model and SRB observations, during DJF. The region in the western tropical Pacific referenced in the text is also shown.
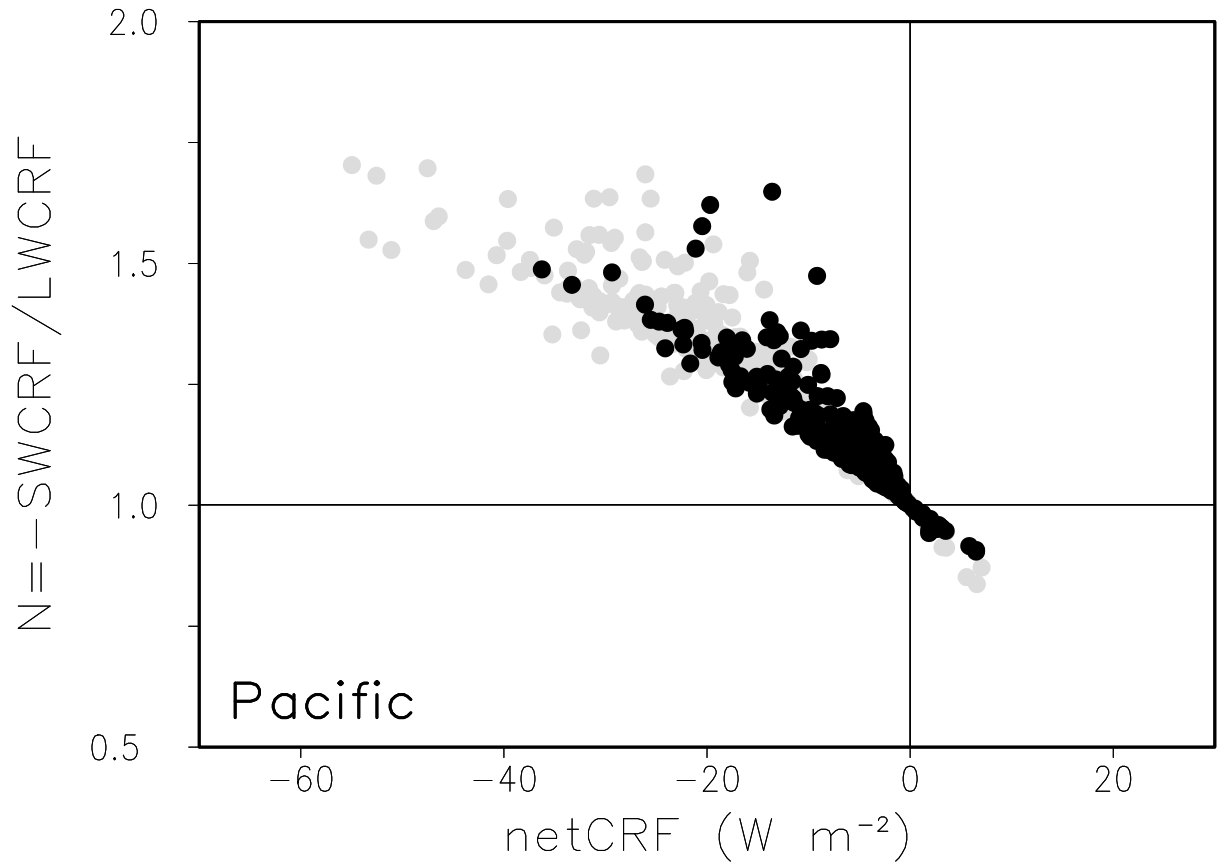
FIG. 11. Scatter plot of $N \times netCRF$ from SRB satellite derived observations (black) and NEW model (gray), for DJF. Each point corresponds to a grid point over the tropical western Pacific region (10°N to 5°S and 117.5°E to 170°E).
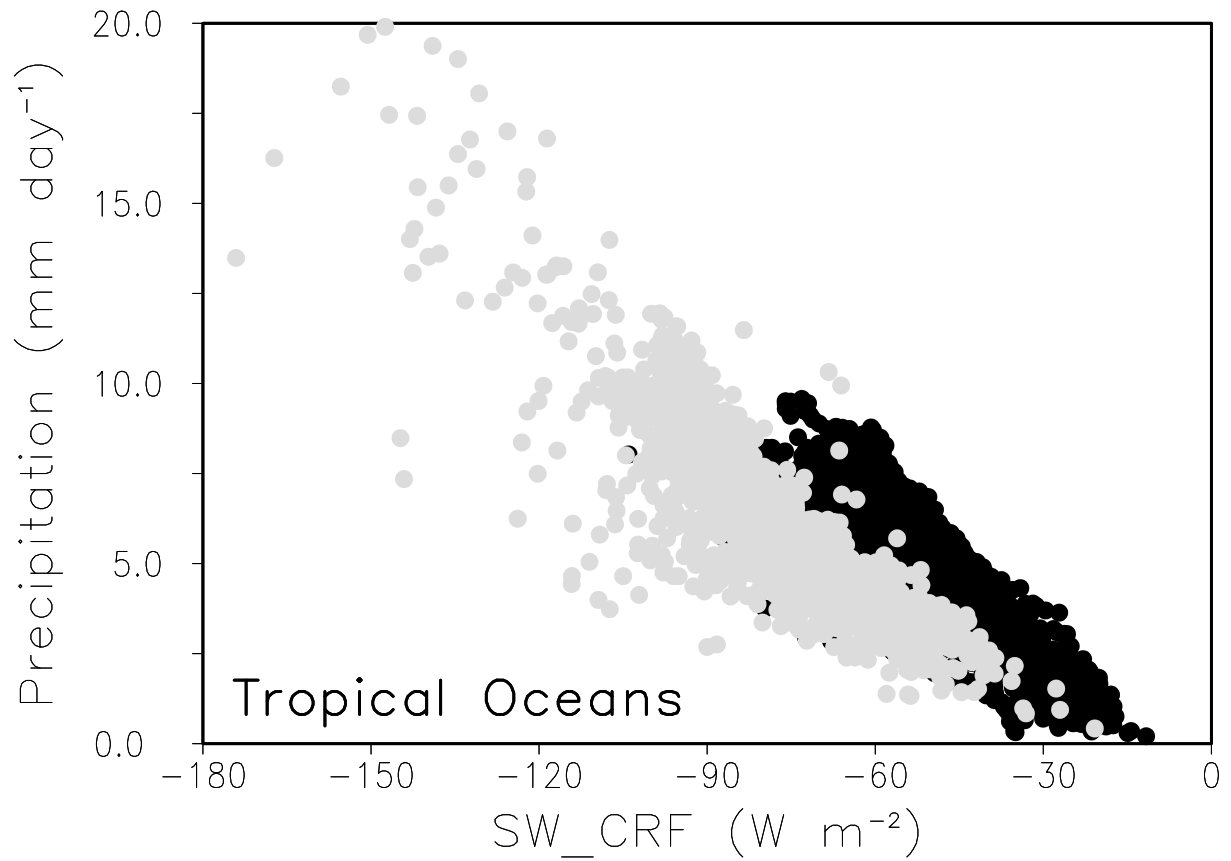
FIG. 12. Scatter plot of convective precipitation versus SWCRF over tropical oceans (20°S–20°N) with annual mean SST>27°C. Observations from SRB and GPCP (black) and NEW model (gray) annual means are shown.
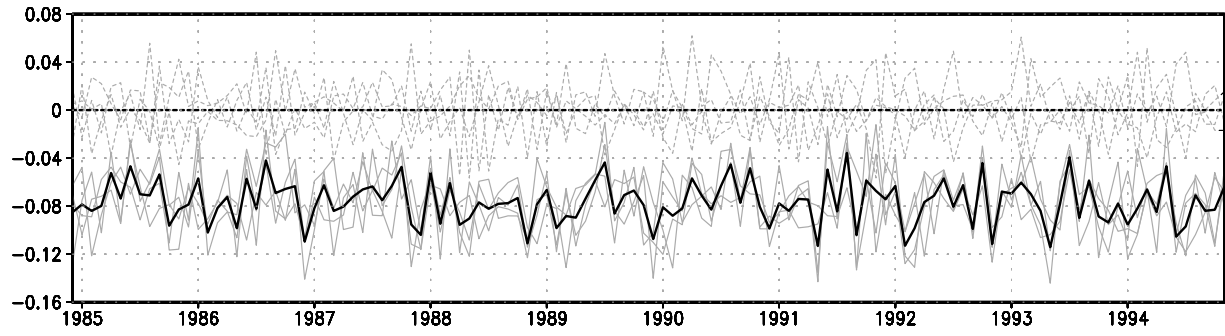
FIG. 13. Global mean precipitation difference between individual model runs and the ensemble of OPE model runs (mm day^{-1}). Integrations with the OPE and NEW models are drawn as dotted and full gray lines respectively. The ensemble means are drawn as thick black lines.
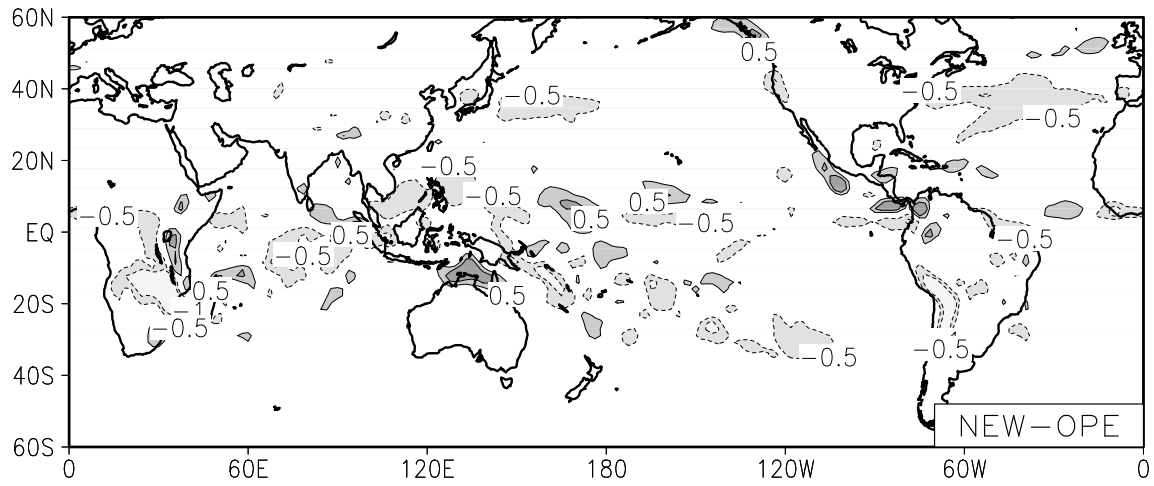
FIG. 14. Improvement in the DJF precipitation distribution shown as the difference in DJF precipitation (mm day^{-1}) between NEW and OPE models.
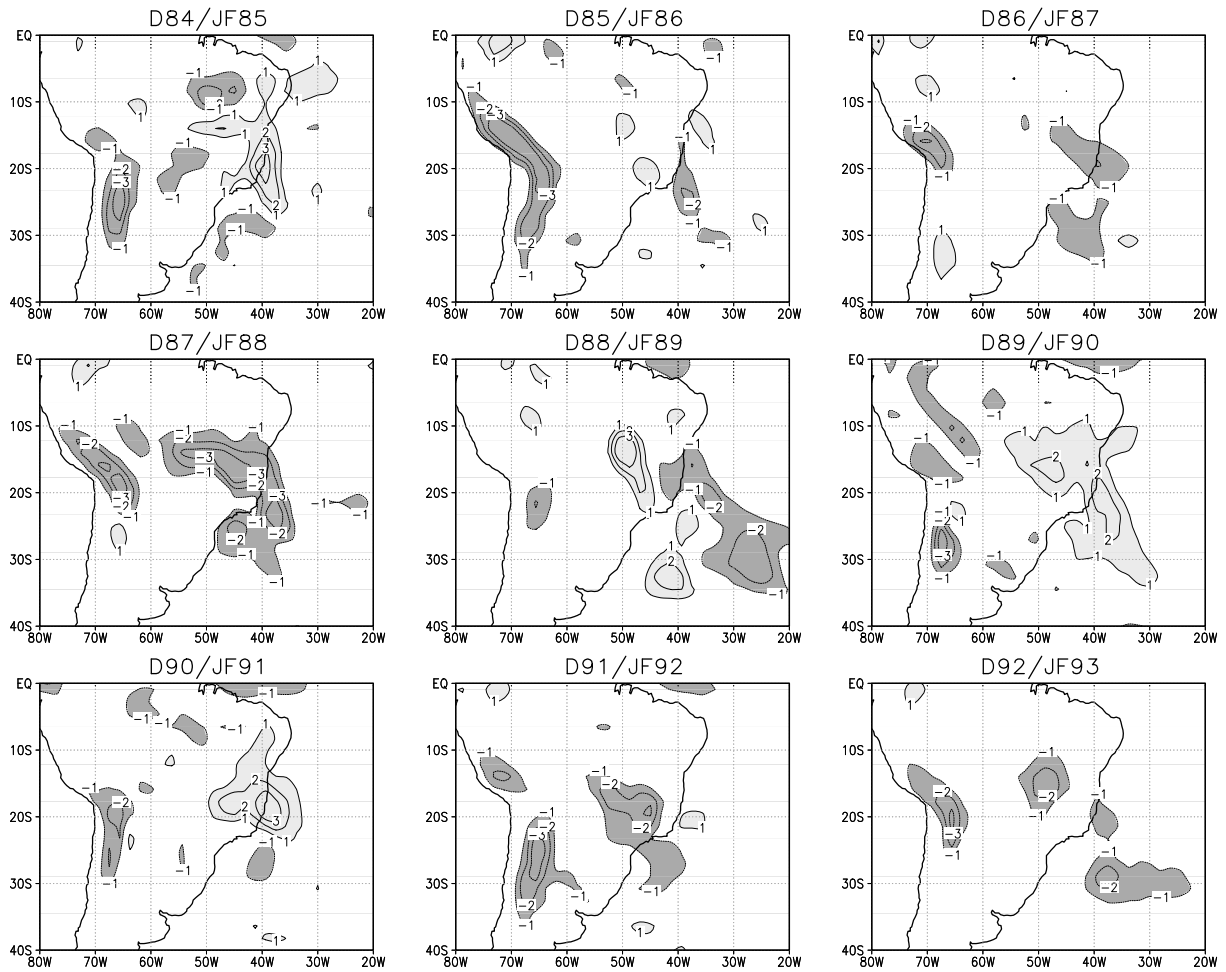
FIG. 15. Changes in the DJF precipitation distribution for the first nine DJF periods. The difference in DJF precipitation (mm day^{-1}) between NEW and OPE models is shown.

50

List of Tables

TABLE 1. The global average of solar radiation absorption ($W\,m^{-2}$), cloud radiative forcing (CRF, $W\,m^{-2}$) and albedo (0-1) are presented. Results for OPE and NEW models, satellite-derived observations from SRB datasets and multi-model means and standard deviations from Wild (2005) and Wild et al. (2006) are shown for all-sky and clear-sky conditions. Results from the experiments with the NEW model without aerosols and water vapor continuum (N-WA) and without aerosols (N-A) are also shown.

	OPE	N-WA	N-A	NEW	SRB	Wild
all-sky absorption						
TOA	244	244	244	241	241	236±6.5
ATM	63	63	64	68	74	74±7.3
SFC	181	181	180	173	167	162±8.4
clear-sky absorption						
TOA	298	296	297	291	288	290±3.9
ATM	63	64	68	72	70	67±4.6
SFC	236	232	229	219	218	222±6.8
TOA SW CRF	-54	-53	-52	-50	-47	-54±1.7
SFC albedo	.11	.11	.11	.11	.13	n/a
TOA albedo	.31	.31	.30	.31	.32	.31±.01

TOA: at the top of the atmosphere

ATM: in the atmosphere

SFC: at the surface.

TABLE 2. Same as Table 1, but for ocean and land separately.

	Ocean					Land				
	OPE	N-WA	N-A	NEW	SRB	OPE	N-WA	N-A	NEW	SRB
all-sky absorption										
TOA	254	254	255	251	251	218	218	219	216	216
ATM	64	64	66	67	73	57	57	60	70	78
SFC	190	190	189	184	179	161	161	159	146	138
clear-sky absorption										
TOA	315	313	313	307	303	256	255	256	252	251
ATM	64	66	70	71	67	57	59	62	75	78
SFC	251	247	243	236	236	199	196	194	177	173
TOA SW CRF	-61	-59	-58	-56	-52	-38	-38	-38	-36	-36
SFC albedo	.06	.06	.06	.06	.09	.25	.25	.25	.25	.23
TOA albedo	.29	.29	.28	.30	.30	.36	.36	.35	.36	.36

TOA: at the top of the atmosphere; ATM: in the atmosphere; SFC: at the surface.